Structural Response to Non-Stationary Thunderstorm Outflows

DAE KUN KWON[1,2], GIOVANNI SOLARI[3], AHSAN KAREEM[1]

[1] *NatHaz Modeling Laboratory, University of Notre Dame, Notre Dame, IN 46556.*

[2] *Center for Research Computing (CRC), University of Notre Dame, Notre Dame, IN 46556.*

[3] *Department of Civil, Chemical and Environmental Engineering, Polytechnic School, University of Genoa, Genoa, Italy, *corresponding author, giovanni.solari@unige.it*

Abstract:

The mechanics associated with thunderstorm outflows differ significantly from traditional turbulence in boundary layer winds both in its kinematics and dynamics. The key distinguishing attributes are the contrasting velocity profile with height, a rapid increase in speed and the statistical features of the energetic gusts in the wind field, exhibiting a strong non-stationarity. This raises serious questions regarding the applicability of conventional stationary process-based theories, thus calling for a paradigm shift. This paper reviews popular approaches concerning the structural analysis of non-stationary thunderstorm outflows, such as evolutionary power spectrum-based analysis, wavelet-based analysis, thunderstorm response spectrum technique involving the equivalent wind spectrum, and hybrid simulation-based analysis in the time domain. Finally, some preliminary comparisons between the results obtained using these different methods are presented.

Keywords: Evolutionary power spectrum, Numerical simulation, Response spectrum, Stochastic dynamics, Thunderstorm outflow, Time-domain analysis, Time-frequency analysis, Wavelet analysis.

1. Introduction

The study of thunderstorm outflows and their loading on structures is a topic of significant interest in wind engineering [1, 2]. Thunderstorms are mesoscale atmospheric phenomena that consist of a set of storm cells that evolve in about 30 minutes over a few kilometers of space [3]. These give rise to intense transient downdrafts that impact the earth's surface followed by radial outflows with a typical "nose" profile [4, 5] and horizontal ring vortices. The ensemble of these air movements is called "downburst" (Figure 1) and is divided into macro-burst and micro-burst depending on whether its size is greater or smaller than 4 km [3]. The design wind velocity is often related to intense micro-bursts.

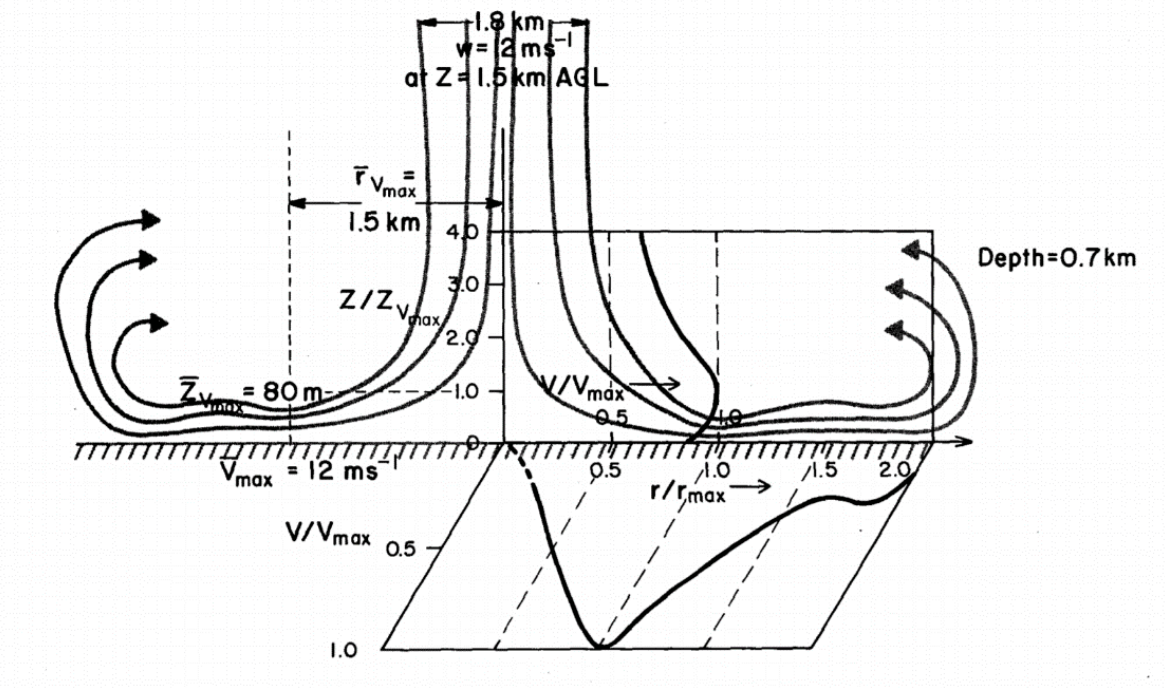

Fig. 1: Thunderstorm downburst and nose velocity profile in the radial outflow [5].

The literature is rich in contributions aiming to determine the dynamic response of reference systems and real structures to thunderstorm outflows. It exhibits an extensive panorama of methods whose complexity matches the complexity of these phenomena. Many other papers did not reach

the evaluation of the wind-induced response but provide propaedeutic methods to represent transient wind fields in the time-domain.

The study of Single-Degree-Of-Freedom (SDOF), Multi-Degree-Of-Freedom (MDOF) and slender beam models are aimed at depicting the conceptual aspects of the structural response, formulating general procedures to evaluate it and to identify the role of the parameters on which the response depends.

In 2002, Choi and Hidayat [6] studied for the first dynamic alongwind response of a SDOF system, aiming to extend the gust factor technique [7] from synoptic to transient winds. This method was refined in [8], where a so-called "Maximum Dynamic Magnification Factor" was defined as the ratio between the maximum dynamic response and the static response to the peak load, and in [9], where ARMA simulations were used to determine a "Dynamic Response Factor" given by the ratio between the maximum response to a downburst and a stationary wind. All these papers solved the linear equations of motion in the time-domain, schematizing the turbulence as identically coherent on the structural surface exposed to the wind loading.

In 2008, Chen [10] performed a frequency domain analysis of the wind-excited response of buildings to nonstationary winds, expressing the wind loading as the sum of a deterministic mean function, slowly-varying with time, and a random fluctuating component, rapidly-varying with time. The response was determined in turn as the sum of a static response to the mean wind loading and a fluctuating response expressed by an evolutionary power spectrum (EPS).

Kwon and Kareem [11] applied the EPS to extend the gust factor method from synoptic winds to gust fronts. They determined the equivalent static force on a building as the product of the equivalent static force associated with an ABL profile, the gust front factor, and a factor that transforms the ABL shape of the force into the gust front shape. The gust front factor was given in turn by the product of the kinematic effects factor, the pulse dynamic factor, the structural dynamics factor, and the load magnification factor. They take into account, respectively, the different profiles of a gust front and an ABL wind, the variation of the mean wind speed, the non-stationary role of

turbulence, and transient aerodynamic effects; the discussion on the latter quantity was purely conceptual.

Also, Huang et al. [12] expressed the nonstationary wind loading by its equivalent power spectral density (EPSD) and simulated nonstationary loading time-histories for integrating the equations of motion in time-domain; results were compared with those obtained in [10]. More recently, Huang et al. [13] advanced a data-driven simulation of multivariate nonstationary winds using a hybrid multivariate empirical mode decomposition and spectral representation method In this context, Zhao et al. [14] presented a fast convolution integration-based scheme for the nonstationary analysis of linear and nonlinear structures with nonproportional damping. Chen [15] developed a frequency-domain framework to predict the multimodal coupled buffeting response of long-span bridges to nonstationary winds. The time-varying mean, self-excited and buffeting forces were modeled respectively by static force coefficients, flutter derivatives, and aerodynamic admittances. Kareem et al. [16] generalized Davenport's chain from stationary to non-stationary winds, based on both wavelet transforms and EPS. This formulation reduces seamlessly to conventional Davenport's chain for stationary cases.

Diversely from EPS and Wavelet techniques, the study of the thunderstorm response of structures carried out at the University of Genova was inspired by the consideration that thunderstorm outflows are transient phenomena with short duration and the structural response to these phenomena, most notably to earthquakes, is usually evaluated by the response spectrum technique [17]. Based on this remark and some previous studies on synoptic winds [18], a "new" method was formulated that generalized the "old" response spectrum technique from earthquakes to thunderstorm outflows.

Initially, this problem was formulated for an SDOF system [19] subjected to a perfectly coherent wind field. This led to express the equivalent static force as the product of the peak wind force by a non-dimensional quantity, the thunderstorm response spectrum, depending on the fundamental frequency and the damping ratio.

Later, this formulation was generalized to MDOF systems [20] subjected to a partially coherent wind field; the structure was modeled as a slender vertical cantilever beam whose dynamic response was dependent on the sole fundamental mode. Analyses were carried out making recourse to the equivalent wind spectrum technique [21], which makes the application of the response spectrum straightforward. The equivalent static force was expressed as the product of the peak wind force by a non-dimensional quantity, the equivalent response spectrum, depending on the first natural frequency, the damping ratio and a reference structural size that synthesizes the role of aerodynamic admittance.

In parallel with the thunderstorm response spectrum technique, time-domain analyses were carried out based on a so-called hybrid simulation strategy [22]. This study showed that the probability density function of the maximum value of the structural response due to thunderstorm outflows is more spread than that related to synoptic extra-tropical cyclones. Thus, diversely from synoptic winds [23], it is not appropriate to identify the maximum response with its mean value. On the other hand, many aspects of the response of structures to thunderstorm outflows are qualitatively similar to synoptic winds: the structural displacement is almost unaffected by the contribution of higher vibration modes; the aerodynamic admittance gives rise to analogous effects for thunderstorms and cyclones; the resonant part of the response to thunderstorms is apparent despite their short duration.

Solari and De Gaetano [24] carried out a joint calibration and advancement of the two methods described above, proving that the results provided by the response spectrum technique and the time-domain solutions closely agree. This confirms the potential of the response spectrum to be a suitable tool for evaluating the thunderstorm loading and response of structures and the efficiency of hybrid simulation and time-domain integrations to study, with a limited computational burden, advanced structural issues. In particular, relevant conceptual and numerical simplifications may be obtained by embedding the equivalent wind spectrum technique [21] within the above non-stationary formulation. It leads to generate a multi-variate non-stationary wind field through the simulation of

a mono-variate stationary process, without any relevant loss of precision.

Within this framework, it is worth mentioning the first research [25] aiming to study the dynamic response taking into account the directional shift of the outflow due to the translation of the thunderstorm cell. It proves that such a shift often involves a relevant increase in the response.

Several other contributions were addressed to the dynamic response of structures to thunderstorm outflows making recourse to different approaches. Le and Caracoglia [26-27] used the Wavelet-Galerkin method to determine the non-linear and/or non-stationary response of SDOF and MDOF systems. Su et al. [28] analyzed the dynamic response of a tall building by a quasi-static approach for the slowly-varying mean and the pseudo-excitation method for the fluctuating component. Wang et al. [29] found a closed-form solution for the buffeting response of a nonlinear double-hinged overhead transmission conductor. Le and Caracoglia [30] implemented a numerical model of the transient response of a tall building under a digitally simulated downburst consistent with an EPS schematization. Peng et al. [31] developed an EPS approach including a time-varying coherence function.

Contrary to complex formulations, Miguel et al. [32] provided a simple engineering model and several critical remarks on the wind loading of buildings due to thunderstorm outflows. Their study confirmed observations previously reported that high-rise buildings are sensitive to extra-tropical cyclones; whereas low-rise buildings are to downbursts.

Finally, it is worth mentioning two papers addressed to structural safety and performance-based design, which used Wavelet-Galerkin method to evaluate structural fragility due to downbursts [33] and combined different features to construct a model that takes into account the non-stationary response to downbursts, wind-induced damage, and costs related to structural maintenance [34].

The contributions described above highlight a wide range of formulations aiming to extend classical stationary structural analyses to non-stationary phenomena. A dominant aspect of many of these contributions is the striking contrast between elegant methods and the lack of data to calibrate and validate these models. The European Projects “Wind and Ports” [35] and “Wind, Ports and

Sea" [36] offer a huge amount of data that provides a unique chance to formulate methods robustly coherent with real measurements. In this framework, an extensive wind monitoring network was created in the High Tyrrhenian area, from which many records of thunderstorm outflows were gathered [37]. Such records were analyzed first aiming to evaluate their statistical properties [38-39], then to develop criteria to determine the loading and response of structures, in particular the thunderstorm response spectrum technique [19-20, 24] and the hybrid simulation strategy [22, 24].

After this brief introduction, Section 2 provides the traditional wind velocity model of thunderstorm outflows. Sections 3 and 4 illustrate, respectively, the Evolutionary Power Spectrum-based analysis and the Wavelet-based analysis. Section 5 describes the thunderstorm response spectrum technique. Section 6 examines the hybrid simulation strategy. Section 7 provides some preliminary comparisons between the results obtained using these different methods. Section 8 summarizes the main conclusions.

2. Wind Velocity Model

The horizontal component of the wind velocity in a thunderstorm outflow (Figure 1) along a vertical axis is expressed here by the classical decomposition rule [40-41]:

$$v(z,t) = \overline{v}(z,t) + v'(z,t) \tag{1}$$

$$v'(z,t) = \sigma_v(z,t)\tilde{v}'(z,t) \tag{2}$$

where z is the height above ground, $t \in [0, \Delta T]$ is the time, ΔT = 10 minutes, $\overline{v}$ is the slowly-varying mean wind velocity, v' is the residual non-stationary fluctuation, σ_v is the slowly-varying standard deviation of v', $\tilde{v}'$ is the reduced turbulent fluctuation dealt with as a stationary Gaussian random field with zero mean and unit standard deviation. The extraction of $\overline{v}$ from v and of σ_v from v' is often carried out here by a moving average filter with an average period T = 30 s [38]; many other methods are available in the literature to perform the same operation in a refined advanced way [42-42]. Replacing Eq. (2) into Eq. (1):

$$v(z,t) = \overline{v}(z,t)\left[1 + I_v(z,t)\tilde{v}'(z,t)\right] \quad (3)$$

where I_v is the slowly-varying turbulence intensity:

$$I_v(z,t) = \frac{\sigma_v(z,t)}{\overline{v}(z,t)} \quad (4)$$

The decoupling of space and time in $\overline{v}$ and I_v allows us to express these two quantities as:

$$\overline{v}(z,t) = \overline{v}_{\max}(h)\alpha(z)\gamma(t) \quad (5)$$

$$I_v(z,t) = \overline{I}_v(z)\beta(z)\mu(t) \quad (6)$$

where $\overline{v}_{\max}$ is the maximum value of $\overline{v}$ in ΔT; h is a reference height; α is a non-dimensional function of z that defines the shape of the vertical profile of $\overline{v}$ [44-46], being $\alpha(h) = 1$; γ is a non-dimensional function of t that expresses the time variation of $\overline{v}$, being $\gamma_{max} = 1$. Similarly, $\overline{I}_v$ is the average value of I_v in ΔT; β is a non-dimensional function of z that defines the shape of the vertical profile of $\overline{I}_v$, being $\beta(h) = 1$; μ is a non-dimensional function of t that expresses the time variation of I_v, being $\overline{\mu} = 1$.

The reduced turbulent fluctuation $\tilde{v}'$ is identified by its cross-power spectral density (CPSD) frequently expressed by the classical models usually adopted for synoptic winds, e.g. [47]:

$$S_{\tilde{v}'}(z,n) = \frac{6.868L_v(z)/\overline{v}_{\max}(z)}{\left[1 + 10.302nL_v(z)/\overline{v}_{\max}(z)\right]^{5/3}} \quad (7)$$

$$Coh_{\tilde{v}'\tilde{v}'}(z,z',n) = \exp\left\{-\frac{2nc_z\left|z - z'\right|}{\overline{v}_{\max}(z) + \overline{v}_{\max}(z')}\right\} \quad (8)$$

where L_v is the integral length scale and c_z is the exponential decay coefficient of $\tilde{v}'$.

Replacing Eqs. (5) and (6) into Eq. (3):

$$v(z,t) = \overline{v}_{\max}(h)\alpha(z)\gamma(t)\left[1 + \overline{I}_v(h)\beta(z)\mu(t)\tilde{v}'(z,t)\right] \quad (9)$$

A novel directional decomposition rule has been recently proposed in [48].

3. Evolutionary Power Spectrum-based analysis

In a non-stationary wind velocity model (Eqs. 1, 2), one of popular representation concerning non-stationary turbulent fluctuation is the introduction of the evolutionary power spectrum (EPS) [e.g., 9-11, 16, 20, 22, 24, 40, 49-62]. In this approach, Eq. (2) is recast in the time-frequency domain in terms of the EPS:

$$G_{\tilde{v}'}(z,n,t) = \left|A(z,n,t)\right|^2 S_{\tilde{v}'}(z,n,t) \tag{10}$$

where $G_{\tilde{v}'}(z,n,t)$ is the longitudinal EPS; $A(z,n,t)$ is the modulating function; $S_{\tilde{v}'}(z,n,t)$ is the longitudinal zero-mean Gaussian process. Besides, amplitude modulating function, which is independent of frequency, and time-independent spectral form (e.g., Eq. 10) are often introduced for simplicity:

$$G_{\tilde{v}'}(z,n,t) = \left|A(z,t)\right|^2 S_{\tilde{v}'}(z,n) \tag{11}$$

With the format in Eq. (11), cross-EPS is expressed in terms of time-independent coherence function (e.g., Eq. 8), akin to the case of boundary layer winds:

$$G_{\tilde{v}'}(z,z',n,t) = \left|A(z,t)\right|^2 \left|A(z',t)\right|^2 S_{\tilde{v}'}(z,n,t) S_{\tilde{v}'}(z',n,t) Coh_{\tilde{v}'\tilde{v}'}(z,z',n) \tag{12}$$

Note that the modulating function is generally assumed to use the decoupling of space (z) and time (t) like Eq. (5), thus it may be expressed as a product of $A(z)$ and $A(t)$.

The structural response in the format of the EPS may be computed from: a) simulation-based approach in the time domain, e.g., invoking Monte Carlo simulation to generate a series of wind load samples and integrate the equations of motion; b) fully non-stationary solution by the direct integration method [e.g., 16, 63-64]; c) computationally efficient solutions such as modal superposition and stochastic decomposition [e.g., 65-66], pseudo excitation method [e.g., 16, 67], etc.; d) approximate closed-form solutions such as the gust front factor framework [11, 55, 62], thunderstorm response spectrum technique [19-20, 24]. In particular, the use of the evolutionary power spectrum offers an advantage for possibly deriving approximate and simplified closed-form

solutions, e.g., gust front factor and thunderstorm response spectrum technique frameworks, which may pave a way towards a codification concerning thunderstorm outflows.

4. Wavelet-based analysis

Wavelet transform is one of the popular time-frequency tools, which can be used as an alternative formulation to heal with non-stationary fluctuating components. Unlike the EPS that compromises the resolutions due to the fixed analysis window size, the wavelet transform adopts flexible windows and thus can achieve the finest time-frequency resolution allowed by Heisenberg's uncertainty principle for all different frequency bands [e.g., 68]. In addition, the wavelet scale can be directly related to the Fourier frequency.

A formulation using the periodic generalized harmonic wavelet (PGHW) is introduced here, in which the wavelet function is defined as [e.g., 16, 69-70]:

$$\Psi^{G}_{(m_j,n_j),k}(t) = \frac{1}{(n-m)} \sum_{q=m_j}^{n_j-1} e^{-iq2\pi\Delta f\left(t-\frac{kT_0}{n-m}\right)} \tag{13}$$

so that wavelet coefficients can be obtained by the wavelet transform:

$$W^{G}_{(m_j,n_j),k}(x) = \frac{n-m}{T_0}\int_0^{T_0} x(t)\Psi^{G}_{(m_j,n_j),k}(t)dt \tag{14}$$

where $x(t)$ is the displacement; $T_0 = N_0\Delta t$ is the time period of concern; $j = 1, \ldots, N_f$; $N_f = N_0/(n-m)$ is the jth wavelet scale and the number of scales; $k, l = 0, \ldots, N_T - 1$; $N_T = (n-m) = n_j - m_j$ is the wavelet time shift and the number of shifts. The equations of motion may be solved in terms of the PGHW, resulting in the wavelet scalogram of response

$$E\left[\mathbf{W}^j_{\mathbf{X}}\left(\mathbf{W}^j_{\mathbf{X}}\right)^T\right] = \left(\frac{T_0}{n-m}\right)^2 \left[\left(\mathbf{A}^j\right)^{-1}\right]\left\{E\left[\mathbf{W}^j_{\mathbf{F}}\left(\mathbf{W}^j_{\mathbf{F}}\right)^T\right]\right\}\left[\left(\mathbf{A}^j\right)^{-1}\right]^T \tag{15}$$

where $\mathbf{W}^j_{\mathbf{X}}$ and $\mathbf{W}^j_{\mathbf{F}}$ are vectors of wavelet coefficients of non-stationary fluctuating response and external force respectively; $\mathbf{A}^j$ is a matrix comprised of block matrix $\mathbf{A}^j_{k,l} = C^{(2)}_{j;k,l}\mathbf{M} + C^{(1)}_{j;k,l}\mathbf{C} + C^{(0)}_{j;k,l}\mathbf{K}$; **M**, **C**, and **K** are mass, damping, and stiffness matrices, respectively; $C^{(o)}_{j;k,l}$ are wavelet connection

coefficients. Detailed information can be found in [69-70]. Eq. (15) implies a wavelet-based representation of second-order structural dynamics system, therefore by analogy, it may be extended to higher-order linear systems. Accordingly, the aerodynamics transfer relationship between non-stationary fluctuating winds and attendant force may also be represented in terms of wavelet coefficients, when this relationship can be approximated by a high-order linear system with sufficient accuracy.

The wavelet scalogram of buffeting response may be transformed into the evolutionary power spectrum (EPS) by:

$$E\left[\mathbf{W}_{\mathbf{x}}^{j}\left(\mathbf{W}_{\mathbf{x}}^{j}\right)^{T}\right]=\frac{(n-m)}{T}\begin{bmatrix} S_{\mathbf{xx}}(n_j,t_1) & & & 0 \\ & S_{\mathbf{xx}}(n_j,t_k) & & \\ & & \ddots & \\ 0 & & & S_{\mathbf{xx}}(n_j,t_{N_T}) \end{bmatrix} \tag{16}$$

A similar relationship also exists for the external force, $\mathbf{W}_{\mathbf{F}}^{j}$.

Note that another wavelet-based analysis, wavelet-Galerkin method, has recently been introduced for computing the dynamic response of tall buildings subject to thunderstorm/downburst events. It utilizes discrete orthonormal Daubechies wavelets as the basis functions in the Galerkin expansion method [27, 30].

5. Thunderstorm Response Spectrum Technique (TRST)

SDOF system

Let us consider an SDOF system [19] subjected to a perfectly coherent wind field. The equation of motion is given by:

$$m\ddot{x}(t)+c\dot{x}(t)+kx(t)=f(t)=\frac{1}{2}\rho v^{2}(t)AC_{D} \tag{17}$$

where x is the alongwind displacement as a function of time t, m, c, and k are the mass, damping, and stiffness, f is the external force, ρ is the density of air, A is the area exposed to the wind loading, C_D is the drag coefficient. Eq. (17) may be rewritten as:

$$\ddot{d}(t)+2\xi(2\pi n_0)\dot{d}(t)+(2\pi n_0)^2 d(t)=(2\pi n_0)^2 u^2(t) \tag{18}$$

where $u(t)=v(t)/\hat{v}$ is the reduced wind velocity, $d(t)=x(t)/\hat{x}$ is the reduced displacement, $\hat{v}$ is the peak wind velocity, $\hat{x}$ is the peak displacement due to the peak force $\hat{f}$ associated with $\hat{v}$, n_0 is the fundamental frequency, ξ is the damping ratio. Accordingly, let us define the thunderstorm response spectrum as:

$$S_d = d_{max}(n_0,\xi) \tag{19}$$

It is easy to show that the maximum alongwind displacement is given by $x_{max}=\hat{x}\cdot S_d$ whereas the equivalent static force results $f_{eq}=\hat{f}\cdot S_d$. Figure 2 shows the mean value and the coefficient of variation (cov) of the response spectrum as obtained from 93 records of thunderstorm outflows detected by the Wind and Ports project.

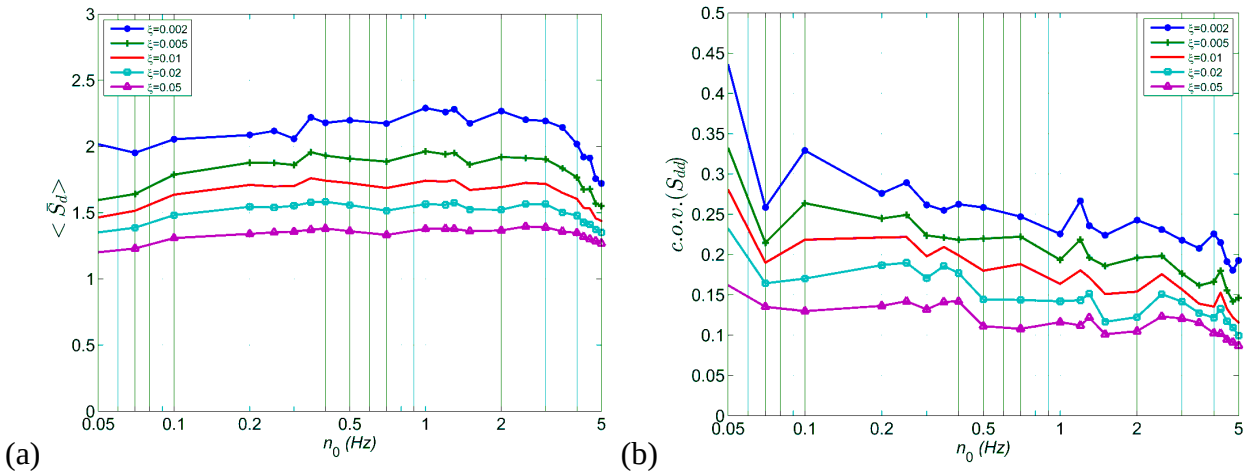

(a) (b)

Fig. 2: Mean value (a) and cov. (b) of the thunderstorm response spectrum.

MDOF system

Let us consider an MDOF system [20] subjected to a partially coherent wind field; for sake of simplicity, the structure is modeled as a slender vertical cantilever beam whose dynamic response depends on the sole fundamental mode with natural frequency n_1. The partially coherent nature of the wind field represents a major difficulty in solving this problem. However, it is overcome by

using the equivalent wind spectrum technique [21] concerning the stationary component, $\tilde{v}'(z,t)$, in Eq. (9). This leads to a new formulation that represents a generalization of the response spectrum technique described above for a SDOF system. Accordingly, Eq. (18) may be re-written as:

$$\ddot{d}_{eq}(t) + 2\xi(2\pi n_1)\dot{d}_{eq}(t) + (2\pi n_1)^2 d_{eq}(t) = (2\pi n_1)^2 u_{eq}^2(\delta,t) \tag{20}$$

where $u_{eq}(\delta,t) = v_{eq}(h,\delta,t)/\hat{v}(h)$ is the reduced equivalent wind velocity, $d_{eq}(t) = x(h,t)/\hat{x}(h)$ is the reduced equivalent displacement, δ is a so-called size factor that takes into account the role of aerodynamic admittance. As a consequence, let us define the equivalent response spectrum as:

$$S_{d,eq} = d_{eq,max}(n_1,\xi,\delta) \tag{21}$$

It is easy to show that the maximum alongwind displacement is given by $x_{max}(z) = \hat{x}(z)\cdot S_{d,eq}$ whereas the equivalent static force results $f_{eq}(z) = \hat{f}(z)\cdot S_{d,eq}$. Figure 3 shows the mean value and the cov of the equivalent response spectrum for ξ = 0.01 as obtained from 93 records of thunderstorm outflows detected by the Wind and Ports project. It is worth noticing that the numerical procedure to solve Eq. (21) is quite elaborated [20] while its application to find the equivalent static force is straightforward.

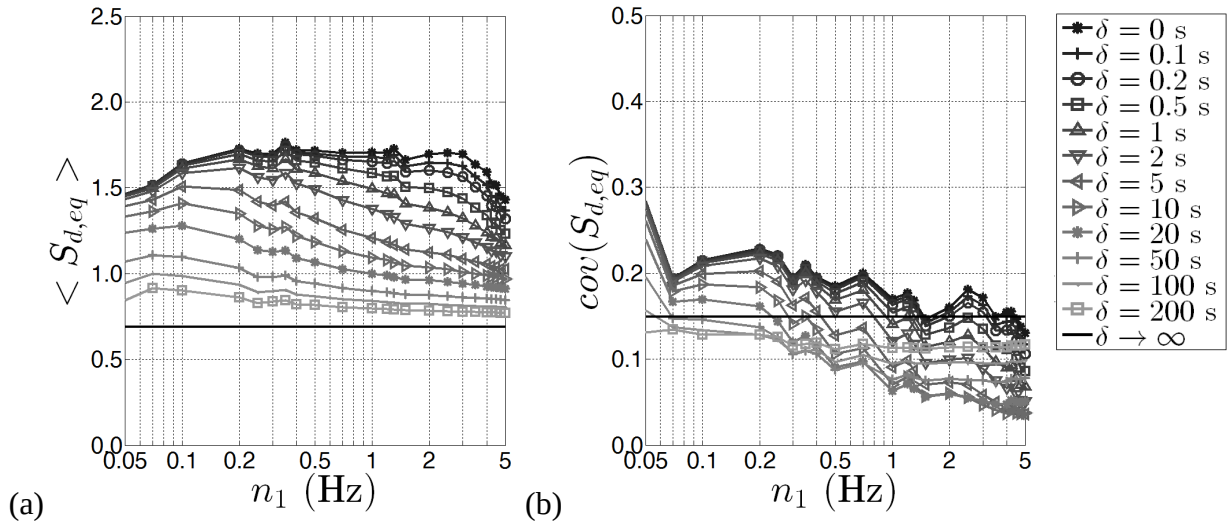

Fig. 3: Mean value (a) and cov. (b) of the equivalent thunderstorm response spectrum for ξ = 0.01.

6. Time-Domain Simulation

Hybrid simulation

Diversely from classical Monte Carlo simulations of non-stationary vector fields [71-74], the hybrid strategy proposed in [22] to generate artificial velocity fields of thunderstorm outflows is based on simulating one at a time and then assembling the different ingredients that make up the wind velocity model in Eq. (9). A brief description of each step is given below.

Step 1: Velocity scale. The maximum value of $\overline{v}$, $\overline{v}_{\max}$, at height h is evaluated by extreme statistics [75] as a function of the return period.

Step 2: Vertical profiles. The vertical profiles of $\overline{v}$ and I_v are evaluated by assigning $\alpha(z)$ and $\beta(z)$ through expressions coherent with measurements. In this paper $\alpha(z)$ is provided by the model proposed in [38] for $J = 4$ values of the height z_m at which $\overline{v}$ is maximum, $z_m = 25, 50, 75, 100$ m; $\beta(z) = 1$ [38].

Step 3: Slowly-varying time dependence. The random time-dependence of $\overline{v}$ and I_v is simulated by gathering measured thunderstorm outflow records [38] and extracting from them synchronous pairs of $\gamma(t)$ and $\mu(t)$ sample functions. For instance, using the data provided by the Wind and Ports monitoring network, $K = 93$.

Step 4: Turbulence field. The space-time variation of the stationary Gaussian field $\tilde{v}'$ is simulated, say L times, by a Monte Carlo algorithm [76] based on the spectral representation method [65, 77]. Its computational efficiency is increased by replacing harmonic superimposition by a Fast Fourier Transform based implementation [65] and by factorizing the PSD matrix of $\tilde{v}'$ by its POD eigenvalues and eigenvectors [78-79]. Typical expressions of the PSD and the coherence function of $\tilde{v}'$ are given by Eqs. 7 and 8 [47].

Step 5: Component assemblage. $M = J \times K \times L$ thunderstorm velocity fields may be simulated for each examined structure. Assuming that each structure is discretized by N nodes, all in all $M \times N$ artificial velocity histories may be generated. Figure 4 shows three sample functions of a wind

velocity field with z_m = 50m. The simulations have been carried out for $\bar{v}_{\max}(h)$ = 36.5 m/s and $L_v(h)$ = 34.6 m, being h = 13 m; c_z = 10. Coherently with measurements, simulations have been carried out with a time step Δt = 0.1 s in a time interval ΔT = 10 minutes. The turbulence harmonic content is simulated between 0 and the cut-off frequency n_c = 5 Hz, with a frequency resolution Δn = 1/600 Hz. L = 1,000 artificial wind fields of $\tilde{v}'$ are simulated for each J = 4 velocity profiles. Therefore, M = $J \times K \times L$ = 4 × 93 × 1,000 = 372,000 thunderstorm velocity fields have been simulated.

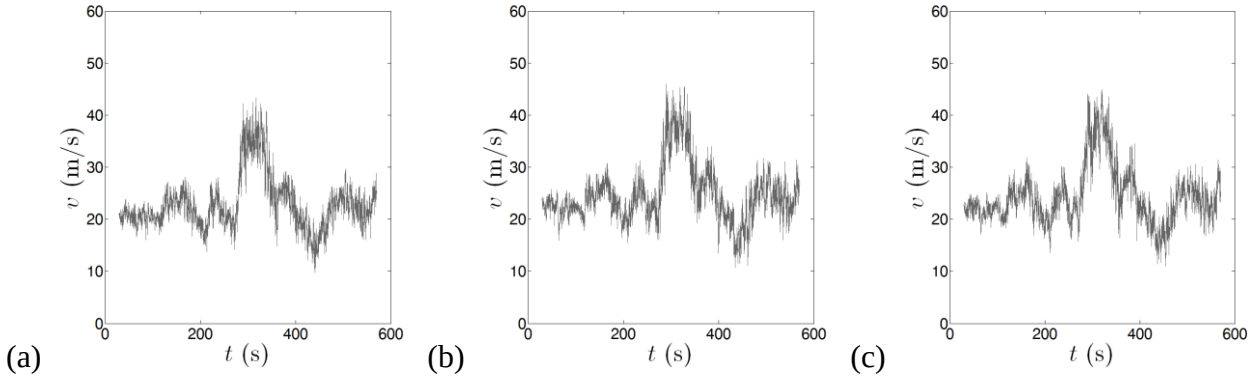

Fig. 4. Sample functions of a wind velocity field v (z_m = 50m) at: a) z = 18m; b) z = 54m; c) z = 80m.

The performance of the whole simulation algorithm has been investigated and discussed in [22], where it was shown that the hybrid technique is characterized by limited errors and produces wind field features consistent with the measured data.

Equivalent hybrid simulation

The equivalent wind spectrum technique described in [21] is a method that replaces the actual turbulent field, as a random function of time and space, by an equivalent turbulent fluctuation, as a random function of time, identically coherent in space.

The generalization of this technique to transient thunderstorm outflows was introduced in [20]. Accordingly, the reduced equivalent turbulent fluctuation $\tilde{v}'_{eq}$ is defined by its PSD:

$$S_{\tilde{v}',eq}(n,\delta) = S_{\tilde{v}'}(z_{eq},n)C(\delta n) \tag{22}$$

where $S_{\tilde{v}'}$ is the PSD of $\tilde{v}'$, z_{eq} = 0.6H is the equivalent height, C is the frequency filter:

$$C(\eta) = \frac{1}{\eta} - \frac{1}{2\eta^2}\left(1 - e^{-2\eta}\right) \quad (\eta > 0)$$
$$C(0) = 1 \tag{23}$$

η is the argument of C; δ is the size factor:

$$\delta = \frac{\kappa c_z H}{\overline{v}_{\max}(z_{eq})} \tag{24}$$

κ is the modal shape factor. Dealing with slender vertical cantilever structures, whose first mode shape may be approximated as $\Psi_1(z) = (z / H)^{\zeta}$, $\kappa = 0.5 / (\zeta + 1)^{0.55}$ [21].

Using this method, Eq. (9) may be approximated by the relationship:

$$v(z,t) = \overline{v}_{\max}(h)\alpha(z)\gamma(t)\left[1 + \overline{I}_v(h)\beta(z)\mu(t)\tilde{v}'_{eq}(t,\delta)\right] \tag{25}$$

Figure 5 shows three sample functions of the equivalent velocity field corresponding to the actual field in Figure 4 (z_m = 50 m). The shape and the trend of the diagrams in Figure 4 are preserved while the high-frequency harmonic content is filtered out to take into account, in equivalent terms, the coherence of the fluctuations and the aerodynamic admittance.

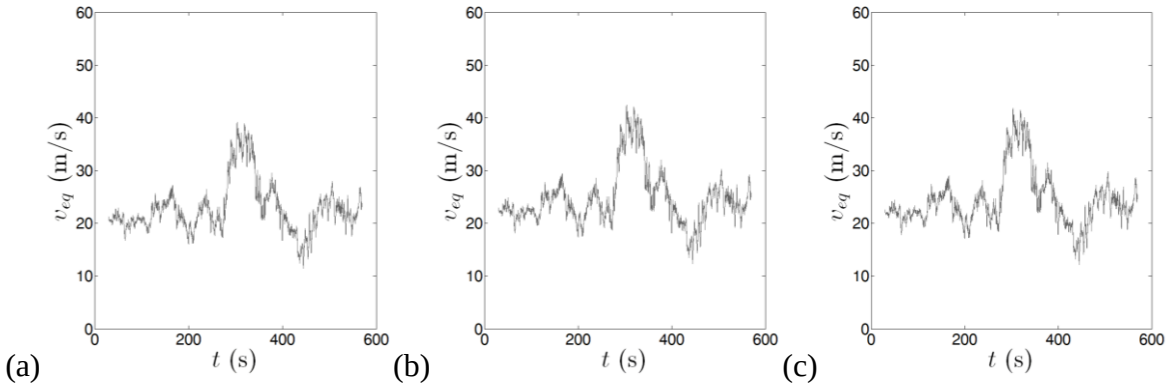

(a) (b) (c)

Fig. 5. Sample functions of the equivalent velocity field v_{eq} corresponding to that in Fig. 4 (z_m = 50 m): (a) z = 18 m; (b) z = 54 m; (c) z = 80 m.

Eq. (25) does not modify the slowly-varying mean part of v whereas it drastically changes its residual fluctuation by replacing the 2-D process $\tilde{v}'(z,t)$ by the equivalent 1-D process $\tilde{v}'_{eq}(t,\delta)$. The step from Eq. (9) to Eq. (25) is a formidable simplification whose correctness was proved conceptually in [24] by stressing that, though used in the non-stationary field, the EWST is strictly applied to the sole stationary part of the turbulent fluctuations.

Wind-excited response

Let us consider a slender vertical structure with linear elastic behavior. Using modal analysis, assuming that natural frequencies are well-separated and dealing with damping as small and proportional, its wind-excited response is given by:

$$x(z,t) = \sum_k \Psi_k(z)\, p_k(t) \tag{26}$$

where Ψ_k is the k-th mode shape and p_k is the k-th principal coordinate:

$$\ddot{p}_k(t) + 2\xi(2\pi n_k)\,\dot{p}_k(t) + (2\pi n_k)^2\, p_k(t) = \frac{1}{m_k}\, f_k(t) \tag{27}$$

m_k and f_k being the k-th modal mass and modal force, respectively:

$$m_k = \int_0^H m(z)\Psi_k^2(z)dz \tag{28}$$

$$f_k(t) = \int_0^H f(z,t)\Psi_k(z)dz \tag{29}$$

in which m is the structural mass per unit length and f is the aerodynamic wind loading:

$$f(t) = \frac{1}{2}\rho v^2(z,t) b(z) C_D(z) \tag{30}$$

where v is the wind velocity defined by Eq. (9) or (25), b is the reference size of the structure cross-section, C_D is the drag coefficient evaluated neglecting the transient character of the wind field [11].

The integration of the equations of motion is conveniently performed in the state space by introducing a Hamming windowing at the beginning of the wind loading history to avoid initial transient effects. Each time step Δt = 0.1 s is divided into 10 parts and a linear interpolation of the

wind loading is applied. Analyses are carried out by neglecting aerodynamic damping and retaining the contribution of the sole first mode.

6. Comparison between Different Methods

To check the consistency of the different methods described above, this section provides some preliminary comparisons between the results obtained using these procedures.

Time-Domain Simulation versus Equivalent Time-Domain Simulation

Three real slender vertical structures are examined here as reference test cases: a steel lighting pole, a steel telecommunication antenna mast, and a reinforced concrete telecommunication tower already studied in [22, 24]. For each of these structures, Figure 6 shows a picture, the model scheme, and the first 3 modal shapes Ψ_1, Ψ_2, Ψ_3. Table 1 reports the main properties: H is the total height; n_1, n_2, n_3 are the first 3 natural frequencies; ξ is the structural damping ratio; N is the number of nodes of the structural model. More details are provided in [24].

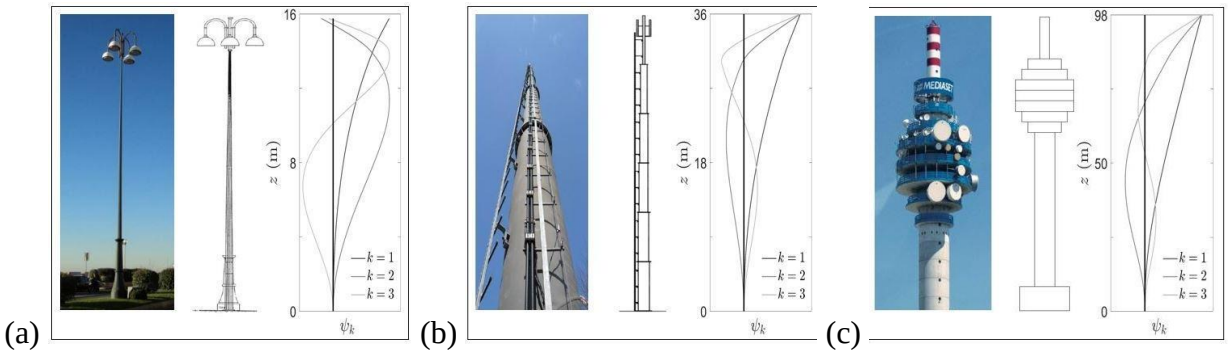

Fig. 6. Structure test cases [24]: a) steel lighting pole (S1); b) steel telecommunication antenna mast (S2); c) reinforced concrete telecommunication tower (S3).

Table 1. Main properties of the three structure test cases.

Structure	Description	H (m)	n_1 (Hz)	n_2 (Hz)	n_3 (Hz)	ξ	N
S1	Steel lighting pole	15.76	0.532	3.186	8.744	0.01	16
S2	Steel telecommunication antenna mast	36.00	0.821	3.106	5.972	0.01	19
S3	R.C. telecommunication tower	98.00	0.494	3.167	6.274	0.02	26

$M = J \times K \times L = 4 \times 93 \times 1{,}000 = 372{,}000$ thunderstorm velocity fields have been simulated for each of the 3 test structures examined. Since they are discretized by N = 16,19,26 nodes (Table 1), all in all, 22,692,000 artificial velocity histories have been generated. Figure 4 shows three sample functions of a wind velocity field with z_m = 50m. Figure 5 shows three sample functions of the equivalent velocity field v_{eq} corresponding to that in Figure 4.

Figures 7 and 8 show the first modal force and the first modal displacement of structure S3 for the simulated thunderstorm outflows in Figures 4 and 5. Despite the first is obtained by Eq. (9) whereas the second derives from the simplified Eq. (25), the similarity between the corresponding diagrams is apparent.

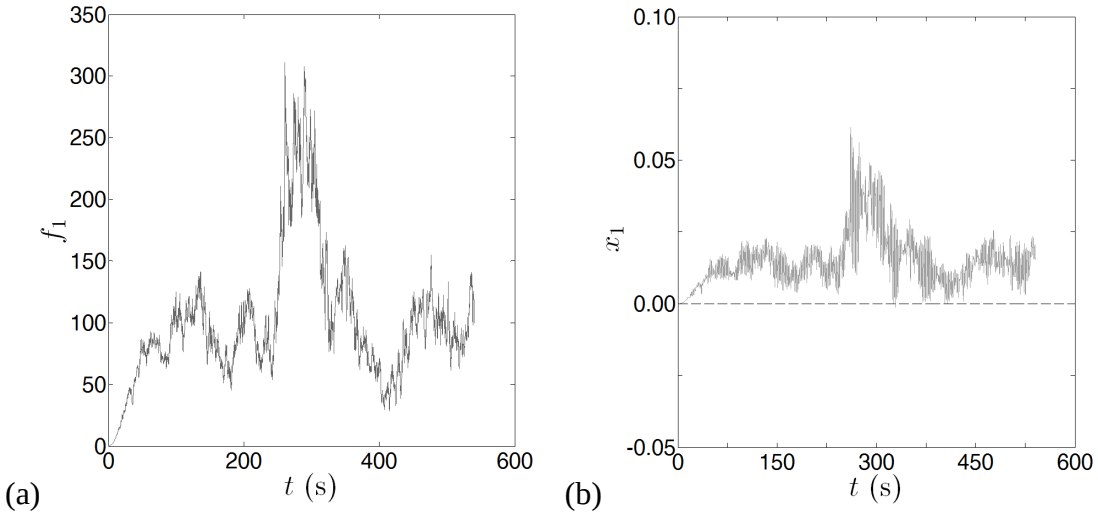

Fig. 7. First modal force f_1 (a) and first modal displacements x_1 (b) of structure S3 for the simulated thunderstorm outflow in Fig. 4.

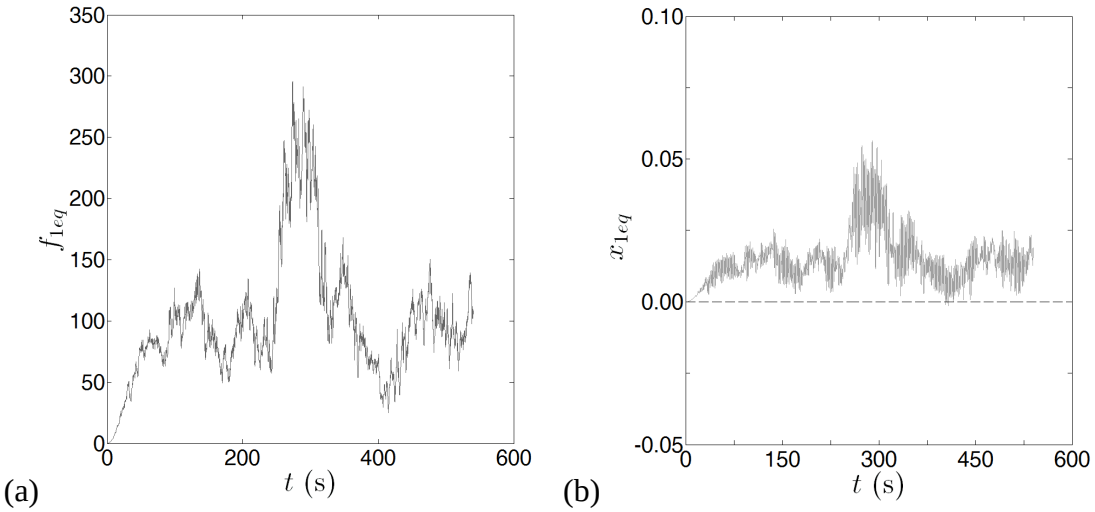

Fig. 8. Equivalent first modal force f_1 (a) and first modal displacements x_1 (b) of structure S3 for a thunderstorm outflow simulated by EWST (Fig. 5).

To check the global efficiency of the equivalent hybrid simulation, 93,000 values of the maximum displacement at the top of each structure are evaluated for the 4 wind velocity profiles considered here. Thus, all in all, 93,000×3×4=1,116,000 values of $x_{max}(H)$ are extracted and analyzed probabilistically. Tables 2 and 3 summarize the mean values and the cov of $x_{max}(H)$ evaluated, respectively, by the hybrid simulation-based upon Eq. (9) and by the equivalent hybrid simulation based upon the approximate Eq. (25). The values in parenthesis are the percent errors committed (with reference to Tables 2). Despite the complexity of the problem dealt with, the error never exceeds 4%. In particular, it is almost surprising the precision with which the EWST replicates not only the mean of $x_{max}(H)$ but also its cov.

Table 2. Mean value (m) and cov of the maximum displacement x_{max} at the structure top H through hybrid time-domain simulation.

Structure	$\langle x_{\max}(H)\rangle$				$\mathrm{cov}(x_{\max}(H))$			
	z_m = 25m	z_m = 50m	z_m = 75m	z_m = 100m	z_m = 25m	z_m = 50m	z_m = 75m	z_m = 100m
S1	0.651	0.651	0.643	0.639	0.242	0.246	0.241	0.240
S2	0.326	0.357	0.364	0.370	0.216	0.218	0.218	0.218
S3	0.046	0.072	0.082	0.087	0.184	0.192	0.195	0.193

Table 3. Mean value (m) and cov of the maximum displacement x_{max} at the structure top H through equivalent hybrid time-domain simulation (in parenthesis the percent error related to Table 2).

Structure	$\langle x_{\max}(H)\rangle$				$\mathrm{cov}(x_{\max}(H))$			
	z_m = 25m	z_m = 50m	z_m = 75m	z_m = 100m	z_m = 25m	z_m = 50m	z_m = 75m	z_m = 100m
S1	0.670 (+3)	0.665 (+2)	0.658 (+2)	0.654 (+2)	0.247(+2)	0.249 (+1)	0.244 (+1)	0.243 (+1)
S2	0.335 (+3)	0.362 (+1)	0.374 (+3)	0.377 (+2)	0.221 (+2)	0.219 (+1)	0.223 (+2)	0.220 (+1)
S3	0.046 (-1)	0.070 (-3)	0.079 (-4)	0.084 (-4)	0.180 (-2)	0.185 (-4)	0.188 (-4)	0.186 (-4)

Time-Domain Simulation versus Equivalent Response Spectrum Technique.

Tables 4 and 5 show respectively the mean value and the cov of the maximum displacement at the top of the reference test structures as evaluated by the equivalent response spectrum technique. The values in parenthesis are the percent errors with respect to hybrid time-domain solution (Tables 3 and 4) treated here as a reference target.

Table 4. Mean value of the maximum displacement x_{max} (m) at the structure top H by the equivalent response spectrum technique (in parenthesis the percent error with reference to Table 3).

Structure	$\xi = \xi_a$				$\xi = \xi_b$			
	z_m = 25m	z_m = 50m	z_m = 75m	z_m = 100m	z_m = 25m	z_m = 50m	z_m = 75m	z_m = 100m
S1	0.630 (-3)	0.624 (-4)	0.622 (-3)	0.620 (-3)	0.783(-8)	0.775 (-9)	0.773 (-8)	0.771 (-7)
S2	0.323 (-1)	0.351 (-2)	0.359 (-1)	0.363 (-2)	0.395 (-5)	0.429 (-6)	0.439 (-6)	0.444 (-6)
S3	0.046 (=)	0.071 (-1)	0.080 (-2)	0.085 (-2)	0.053 (-4)	0.081 (-7)	0.092 (-8)	0.097 (-8)

Table 5. Cov of the maximum displacement x_{max} at the structure top H by the equivalent response spectrum technique (in parenthesis the percent error with reference to Table 4).

Structure	$\xi = \xi_a$				$\xi = \xi_b$			
	z_m = 25m	z_m = 50m	z_m = 75m	z_m = 100m	z_m = 25m	z_m = 50m	z_m = 75m	z_m = 100m
S1	0.169(-30)	0.169(-31)	0.169(-30)	0.169(-30)	0.240(-18)	0.240(-19)	0.240(-17)	0.240(-17)
S2	0.142(-34)	0.143(-34)	0.143(-34)	0.143(-34)	0.199(-23)	0.200(-24)	0.200(-23)	0.200(-24)
S3	0.095(-48)	0.099(-48)	0.100(-49)	0.100(-48)	0.142(-34)	0.149(-34)	0.151(-36)	0.152(-34)

As far as concerns the errors committed by determining the mean value of $x_{max}(H)$ by $\langle S_{d,eq} \rangle$, they are so small that, in their regard, the response spectrum technique can be judged as highly effective. This remark is strengthened by the tremendous conceptual and computational simplifications involved by this technique in comparison to the sequential application of hybrid simulation, even if in its equivalent form, and hybrid time-domain solution. Examining these errors more in detail, for average damping values ($\xi = \xi_a$) they do not exceed 3-4%. For low damping values ($\xi = \xi_b$) errors reach 8-9%. In any case, differently from the hybrid time-domain solution involving the equivalent wind spectrum technique (Table 4), the response spectrum technique underestimates always the structural response. Besides, errors are almost independent of the wind speed profile.

Regarding the errors committed by determining the cov of $x_{max}(H)$ by $\mathrm{cov}(S_{d,eq})$, they are so large (up to 50%) that they cannot be explained other than in relation to conceptual differences between the two methods. An inspection of these conceptual frameworks carried out in [24] highlighted two main reasons capable of justifying such differences: the use of different reference values of the wind speed and of different methods to reconstruct the thunderstorm outflow velocity field starting from individual velocity records. A detailed explanation is given in [24].

Evolutionary Power Spectral Density versus Thunderstorm Response Spectrum Technique.

Recently, Kwon and Kareem [62] compared the EPSD-based gust front factor (GFF/G-GFF) framework with the thunderstorm response spectrum technique (TRST) framework. It was found that while underlying principles between the two frameworks to describe the peak wind load were close following the non-stationary model (Eq. 1), some differences such as the use of the maximum wind velocity and velocity profile, etc. were noticed. Besides, the two frameworks used different approaches for the treatment of nonstationary turbulence components. While the TRST employed data-based equivalent wind velocity approach in the time domain (Eq. 20) for estimating the ERS ($S_{d,eq}$) (Eq. 21), the GFF/G-GFF utilized conventional frequency domain approach involving evolutionary power spectrum model (Eqs. 10-12) in which the spectrum was described as a product of amplitude modulating function and stationary wind component assuming Davenport wind spectrum. To overcome these differences for a comparison, Kwon and Kareem [62] introduced a non-dimensionalized factor normalized by common parameters used in both frameworks for an indirect comparison. In view of all intrinsic differences between the GFF/G-GFF and TRST approaches, they showed reasonably good agreement with each other, i.e., less than 10 % differences. More detailed information can be found in Chapter 7-3.

7. Conclusions

The literature is rich in contributions aiming to determine the dynamic response of structures to transient thunderstorm outflows whose complexity matches the complexity of the phenomenon itself. Several papers did not offer schemes to evaluate the wind-induced response but only provide propaedeutic methods to represent transient wind fields in time-domain. A dominant aspect of many of these contributions is the striking contrast between well-designed methods and the lack of data to calibrate and validate these models.

This chapter deals with the dynamic response of structures to non-stationary thunderstorm outflows with particular regard to single-degree-of-freedom, multi-degree-of-freedom and distributed mass systems. This choice allows focusing attention on the dominant conceptual aspects of the dynamic response of the structures, identifying the main parameters essential to describe the response.

With such a premise, this contribution initially emphasizes the time-frequency domain methods such as the evolutionary power spectrum-based and the wavelet-based approaches, briefly reviewing their respective formulations. In particular, the use of the evolutionary power spectrum offers an advantage for possibly deriving approximate and simplified closed-form solutions, e.g., the gust front factor framework, which may pave a way towards codification of response to thunderstorm outflows.

Subsequently, the chapter illustrates the response spectrum technique popular in the seismic field and recently generalized to thunderstorms. Like the gust front factor method, this procedure also offers ample opportunities for closed-form engineering solutions. The chapter then goes on to discuss a new wind field simulation scheme referred to as a hybrid strategy, and the use of the equivalent spectrum method to significantly reduce the computational burden without compromising the accuracy of results.

In its final part, the paper illustrates a series of applications of the various methods outlined here and compares the results. Clearly preliminary assessment suggest a promising agreement which

may promote interesting engineering developments about the design of structures subjected to thunderstorm outflows.

Acknowledgments

The first and third authors gratefully acknowledge the support in part by the NSF Grant CMMI-1562244. The research carried out by the second author is funded by the European Research Council (ERC) under the European Union's Horizon 2020 research and innovation program (grant agreement No. 741273) for the project THUNDERR - Detection, simulation, modeling and loading of thunderstorm outflows to design wind-safer and cost-efficient structures – supported by an Advanced Grant 2016. The data exploited have been recorded by the monitoring network realized for the European Projects "Winds and Ports" (grant No. B87E09000000007) and "Wind, Ports and Sea" (grant No. B82F13000100005), funded by the European Territorial Cooperation Objective, Cross-border program Italy-France Maritime 2007-2013.

References

1. C.W. Letchford, C. Mans, M.T. Chay, *Thunderstorms – their importance in wind engineering (a case for the next generation wind tunnel)*, J. Wind Eng. Ind. Aerod. 90 (2002) 1415-1433.
2. G. Solari, *Emerging issues and new scenarios for wind loading on structures in mixed climates*, Wind Struct. 19 (2014) 295-320.
3. T.T. Fujita, *Downburst: meteorological features and wind field characteristics*, J. Wind Eng. Ind. Aerod. 36 (1990) 75-86.
4. R.G. Goff, *Vertical structure of thunderstorm outflows*, Mon. Wea. Rev. 104 (1976) 1429-1440.
5. M.R. Hjelmfelt, *Structure and life cycle of microburst outflows observed in Colorado*, J. Appl. Meteorol. 27 (1988) 900-927.
6. E.C.C. Choi, F.A. Hidayat, *Dynamic response of structures to thunderstorm winds*, Prog. Struct. Eng. Mat. 4 (2002) 408-416.

7. A.G. Davenport, *The application of statistical concepts to the wind loading of structures*. Proc. Inst. Civ. Eng. 19 (1961) 449-472.
8. L. Chen, C.W. Letchford, *Parametric study on the alongwind response of the CAARC building to downbursts in the time domain*, J. Wind Eng. Ind. Aerod. 92 (2004) 703-724.
9. M.T. Chay, F. Albermani, B. Wilson, *Numerical and analytical simulation of downburst wind loads*, Eng. Struct. 28 (2006) 240-254.
10. X. Chen, *Analysis of alongwind tall building response to transient nonstationary winds*, J. Struct. Eng. ASCE 134 (2008) 782-791.
11. D.K. Kwon, A. Kareem, *Gust-front factor: new framework for wind load effects on structures*, J. Struct. Eng. ASCE 135 (2009) 717-732.
12. G. Huang, X. Chen, H. Liao, M. Li, *Predicting of tall building response to non-stationary winds using multiple wind speed samples*. Wind Struct. 17 (2013) 227-244.
13. G. Huang, L. Peng, A. Kareem, C. Song, Data-driven simulation of multivariate nonstationary winds: a hybrid multivariate empirical mode decomposition and spectral representation method, J. Wind Eng. Ind. Aerod. 197 (2020) 104073.
14. N. Zhao, G. Huang, Q. Yang, X. Zhou, A. Kareem, Fast convolution integration-based nonstationary response analysis of linear and nonlinear structures with nonpropotional damping, J. Eng, Mech. ASCE 145(8) (2019) 04019053.
15. X. Chen, *Analysis of multimode coupled buffeting response of long-span bridges to non-stationary winds with force parameters from stationary wind*. J. Struct. Eng. ASCE 141 (2015) 04014131.
16. A. Kareem, L. Hu, Y. Guo, D.K. Kwon, *Generalized wind loading chain: Time-frequency modeling framework for non-stationary wind effects on structures*, J. Struct. Eng. ASCE 145 (2019) 04019092.
17. G.W. Housner, R.R. Martel, J.L. Alford, *Spectrum analysis of strong-motion earthquakes*. Bull. Seism. Soc. Am. 43 (1953) 97-119.

18. G. Solari, *Wind response spectrum*. J. Eng. Mech. ASCE 115 (1989) 2057-2073.
19. G. Solari, P. De Gaetano, M.P. Repetto, *Thunderstorm response spectrum: fundamentals and case study*, J. Wind Eng. Ind. Aerod. 143 (2015) 62-77.
20. G. Solari, *Thunderstorm response spectrum technique: theory and applications*, Eng. Struct. 108 (2016) 28-46.
21. G. Piccardo, G. Solari, *Generalized equivalent spectrum technique*, Wind Struct. 1 (1998) 161-174.
22. G. Solari, D. Rainisio, P. De Gaetano, *Hybrid simulation of thunderstorm outflows and wind-excited response of structures*, Meccanica 52 (2017) 3197–3220.
23. A.G. Davenport, *Note on the distribution of the largest value of a random function with application to gust loading*. Proc. Inst. Civ. Eng. London U.K. 24 (1964) 187-196.
24. G. Solari, P. De Gaetano, *Dynamic response of structures to thunderstorm outflows: response spectrum technique vs time-domain analysis*, Eng. Struct. 176 (2018) 188-207.
25. S. Brusco, V. Lerzo, G. Solari, *Directional response of structures to thunderstorm outflows*. Meccanica 54 (2019) 1281–1306.
26. T.H. Le, L. Caracoglia, *Reduced-order Wavelet-Galerkin solution for the coupled, nonlinear stochastic response of slender buildings in transient winds*, J. Sound Vibr. 344 (2015) 179-208.
27. T.-H. Le, L. Caracoglia, *Wavelet-Galerkin analysis to study the coupled dynamic response of a tall building against transient wind loads*, Eng. Struct. 100 (2015) 763-778.
28. Y. Su, G. Huang, Y.L. Xu, *Derivation of time-varying mean for non-stationary downburst winds*, J. Wind Eng. Ind. Aerod. 141 (2015) 39-48.
29. D. Wang, X. Chen, K. Xu, *Analysis of buffeting response of hinged overhead transmission conductor to nonstationary winds*. Eng. Struct. 147 (2017) 567-582.
30. T.H. Le, L. Caracoglia, *Computer-based model for the transient dynamics of a tall building during digitally simulated Andrews AFB thunderstorm*, Comp. Struct. 193 (2018) 44-72.

31. L. Peng, G. Huang, X. Chen, Q. Yang, *Evolutionary spectra-based time-varying coherence function and application in structural response analysis to downburst winds*. J. Struct. Eng. ASCE 144 (2018) 04018078.
32. L.F.F. Miguel, J.D. Riera, L.F.F. Miguel, *Assessment of downburst wind loading on tall structures*. J. Wind Eng. Ind. Aerod. 174 (2018) 252-259.
33. V. Le, L. Caracoglia, *Computationally efficient stochastic approach for the fragility analysis of vertical structures subjected to thunderstorm downburst winds*. Eng. Struct. 165 (2018) 152-169.
34. L. Caracoglia, *Unified stochastic dynamic and damage cost model for the structural analysis of tall buildings in thunderstorm-like winds*. ASCE-ASME J. Risk. Unc. Eng. Syst. 4 (2018) 04018043.
35. G. Solari, M.P. Repetto, M. Burlando, P. De Gaetano, M. Pizzo, M. Tizzi, M. Parodi, *The wind forecast for safety and management of port areas*, J. Wind Eng. Ind. Aerod. 104-106 (2012) 266-277.
36. M.P. Repetto, M. Burlando, G. Solari, P. De Gaetano, M. Pizzo, M. Tizzi, *A GIS-based platform for the risk assessment of structures and infrastructures exposed to wind*, Adv. Eng. Softw. 117 (2018) 29-45.
37. P. De Gaetano, M.P. Repetto, T. Repetto, G. Solari, *Separation and classification of extreme wind events from anemometric records*, J. Wind Eng. Ind. Aerod. 126 (2014) 132-143.
38. G. Solari, M. Burlando, P. De Gaetano, M.P. Repetto, *Characteristics of thunderstorms relevant to the wind loading of structures*, Wind Struct. 20 (2015) 763-791.
39. S. Zhang, G. Solari, P. De Gaetano, M. Burlando, M.P. Repetto, *A refined analysis of thunderstorm outflow characteristics relevant to the wind loading of structures*, Prob. Eng. Mech. 54 (2018) 9-24.
40. L. Chen, C.W. Letchford, *A deterministic-stochastic hybrid model of downbursts and its impact on a cantilevered structure*, Eng. Struct. 26 (2004) 619-629.

41. J.D. Holmes, H.M. Hangan, J.L. Schroeder, C.W. Letchford, K.D. Orwig, *A forensic study of the Lubbock-Reese downdraft of 2002*, Wind Struct. 11 (2008) 19-39.
42. L. Chen, C.W. Letchford, *Numerical simulation of extreme winds from thunderstorm downbursts*, J. Wind Eng. Ind. Aerod. 95 (2007) 977-990.
43. M. Mccullough, D.K. Kwon, A. Kareem, L. Wang, *Efficacy of averaging interval for non-stationary winds*, J. Wind Eng. Ind. Aerod. 140 (2013) 1-19.
44. R.M. Oseguera, R.L. Bowles, *A simple analytic 3-dimensional downburst model based on boundary layer stagnation flow*, NASA Technical Memorandum 100632, 1988.
45. D.D. Vicroy, *Assessment of microburst models for downdraft estimation*, J. Aircraft. 29 (1992) 1043-1048.
46. G.S. Wood, K.C.S. Kwok, *An empirically derived estimate for the mean velocity profile of a thunderstorm downburst*, Proceedings of the 7th Australian Wind Engineering Society Workshop, Auckland, Australia, 1998.
47. G. Solari, G. Piccardo, *Probabilistic 3-D turbulence modeling for gust buffeting of structures*, Prob. Eng. Mech. 16 (2001) 73-86.
48. S. Zhang, G. Solari, M. Burlando, Q. Yang, *Directional decomposition and analysis of thunderstorm outflows*. J. Wind Eng. Ind. Aerod. 189 (2019) 71-90.
49. L. Wang, M. McCullough, A. Kareem, *A data-driven approach for simulation of full-scale downburst wind speeds*, J. Wind Eng. Ind. Aerod. 123 (2013) 171-190.
50. G. Huang, H. Zheng, Y.L. Xu, Y. Li, *Spectrum models for non-stationary extreme winds*, J. Struct. Eng. ASCE 141 (2015) 04015010.
51. L. Peng, G. Huang, X. Chen, A. Kareem, *Simulation of multivariate nonstationary random processes: hybrid stochastic wave and proper orthogonal decomposition approach*, J. Eng. Mech. ASCE 143 (2017) 04017064.
52. M.B. Priestley, *Evolutionary spectra and non-stationary processes*, J. Royal Statistical Society. Series B (Methodological) 27(2) (1965) 204-237.

53. M.B. Priestley, *Power spectral analysis of nonstationary random process* J. Sound Vibr. 6(1) (1967) 86-97.
54. A. Kareem, *Numerical simulation of wind effects: A probabilistic perspective*, J. Wind Eng. Ind. Aerod. 96 (2008) 1472-1497.
55. D. Kwon, A. Kareem, *Gust front factor: new framework for wind load effects on structures*, Eng. Struct. 48 (2013) 635-644.
56. L. Hu, Y.-L. Xu, W.-F. Huang, *Typhoon-induced non-stationary buffeting response of long-span bridges in complex terrain*, Eng. Struct. 57 (2013) 406-415.
57. G.-D. Zhou, Y.-L. Ding, A.-Q. Li, *Evolutionary spectra estimation of field measurement typhoon processes using wavelets*, Mathematical Problems in Engineering (2015), 945203.
58. L. Hu, Y.L. Xu, Q. Zhu, A. Guo, A. Kareem, *Tropical storm-induced buffeting response of long-span bridges: Enhanced non-stationary buffeting force model*, J. Struct. Eng. ASCE 143 (6) (2017) 04017027.
59. H. Wang, T. Wu, T. Tao, A. Li, A. Kareem, Measurements and analysis of non-stationary wind characteristics at Sutong Bridge in Typhoon Damrey." J. Wind Eng. Ind. Aerod. 123 (2016) 100-106.
60. H. Wang, Z. Xu, T. Wu, J. Mao, *Evolutionary power spectral density of recorded typhoons at Sutong Bridge using harmonic wavelets*, J. Wind Eng. Ind. Aerod. 177 (2018) 197-212.
61. H. Wang, Z. Xu, D. Feng, T. Tao, *Non-stationary turbulent wind field simulation of bridge deck using non-negative matrix factorization*, J. Wind Eng. Ind. Aerod. 188 (2019) 235-246.
62. D.K. Kwon, A. Kareem, *Towards codification of thunderstorm/downburst using gust front factor: model-based and data-driven perspectives*, Eng. Struct. 199 (2019) 109608.
63. L.J. Howell, Y.K. Lin, *Response of flight vehicles to nonstationary atmospheric turbulence*, AIAA Journal 9(11) (1971) 2201-2207.
64. J. Li, J. Chen, *Stochastic dynamics of structures*. Singapore: Wiley, 2009.

65. Y. Li, A. Kareem, *Stochastic decomposition and application to probabilistic mechanics*, J. Eng. Mech. ASCE 121 (1995) 162-174.
66. W.-J. Sun, A. Kareem, *Response of MDOF systems to nonstationary random excitation*, Eng. Struct. 11(2) (1989) 83-91.
67. J.H. Lin, *Pseudo excitation method in random vibration*, Beijing: Science Press, 2004.
68. T. Kijewski-Correa, A. Kareem, *Wavelet transforms for system identification in civil engineering*, Comput. Aided Civ. Infrastruct. Eng. 18 (2003) 339–355.
69. F. Kong, J. Li., *Wavelet-expansion-based stochastic response of chain-like MDOF structures*, J. Sound Vib. 359 (2015) 136–153.
70. P.D. Spanos, F. Kong, J. Li, I.A. Kougioumtzoglou, *Harmonic wavelets based excitation-response relationships for linear systems: A critical perspective*, Probab. Eng. Mech. 44 (2016) 163–173.
71. Y. Li, A. Kareem, *Simulation of multivariate nonstationary random processes by FFT*, J. Eng. Mech. ASCE 117 (1991) 1037-1058.
72. G. Deodatis, *Non-stationary stochastic vector processes: seismic ground motion applications*, Prob. Eng. Mech. 11 (1996) 149-168.
73. S. Sakamoto, R. Ghanem, *Simulation of multi-dimensional non-Gaussian non-stationary random fields*, Prob. Eng. Mech. 17 (2002) 167-176.
74. G. Huang, *An efficient simulation approach for multivariate nonstationary process: Hybrid of wavelet and spectral representation method*, Prob. Eng. Mech. 37 (2014) 74-83.
75. S. Zhang, G. Solari, Q. Yang, M.P. Repetto, *Extreme wind speed distribution in a mixed wind climate*, J. Wind Eng. Ind. Aerod. 176 (2018) 239-253.
76. L. Carassale, G. Solari, *Monte Carlo simulation of wind velocity fields on complex structures*, J. Wind Eng. Ind. Aerod. 94 (2006) 323-339.
77. M. Shinozuka, C.M. Jan, *Digital simulation of random processes and its applications*, J. Sound Vibr. 25 (1972) 111-128.

78. M. Di Paola, *Digital simulation of wind field velocity*, J. Wind Eng. Ind. Aerod. 74-76 (1998) 91-109.
79. L. Carassale, G. Solari, F. Tubino, *Proper Orthogonal Decomposition in wind engineering. Part 2: Theoretical aspects and some applications*, Wind Struct. 10 (2007) 177-208.